35th Annual International Conference of the IEEE EMBS
Osaka, Japan, 3 - 7 July, 2013

A Novel Aortic Valve Segmentation from Ultrasound Image Using Continuous Max-Flow Approach

Yuanyuan Nie, Zhe Luo, Junfeng Cai and Lixu Gu*, *Senior Member, IEEE*

***Abstract*— Geometric features of aortic valve can be applied in diagnostic, modeling and image-guided cardiac intervention, however methods to accurately and effectively delineate aortic valve from ultrasound (US) image are not well addressed. This paper proposes a novel aortic valve segmentation algorithm for intra-operative 2D short-axis US image using probability estimation and continuous max-flow (CMF) approach. The algorithm first calculates composite probability estimation (CPE) and single probability estimation (SPE) over 5 prior images based on both intensity and distance to the corresponding centroid, then the energy function for the current input image is constructed, followed by a Graphic Processing Unit (GPU) accelerated CMF approach to achieve aortic valve contours in approximately real time. Quantitative evaluations over 270 images acquired from 3 subjects indicated the results of the algorithm had good correlation with the manual segmentation results (ground truth) by an expert. The Average Symmetric Contour Distance (ASCD), Dice Metric (DM), and Reliability were employed to evaluate our algorithm, and the evaluation results of these three metrics were 1.79±0.46 (in pixels), 0.96±0.01 and 0.84 (d=0.95) respectively, where the computational time was 39.23±5.02 ms per frame.**

I. Introduction

The aortic valve is an important cardiac structure including three leaflets, the geometric features of which are very valuable in many applications, such as clinical diagnostics, modeling applications and image-guided cardiac interventions and therapy, especially in Transcatheter Aortic Valve Implantation (TAVI) [1]. As a routine cardiac imaging modality in clinic, the ultrasound (US) has ability of capturing fast moving valve structures [2]. It is commonly used to visualize intra-operative aortic valve in TAVI [3, 4]. In order to provide accurate image-guidance for TAVI, several works have been done on the registration between intra-operative US image and a model derived from pre-operative computed tomography (CT), in which the segmentation of aortic valve from US image is one of the challenging steps, due to the following degradation factors [5, 6]:

* Corresponding author

This research is partially supported by the Chinese NSFC research fund (61190120, 61190124, 61271318), the Shanghai municipal health bureau research fund (2011216) and Biomedical engineering fund of Shanghai Jiao Tong University (YG2012MS21).

Yuanyuan Nie, Zhe Luo and Lixu Gu are with the Laboratory of Image Guided Surgery and Therapy (IGST), Shanghai Jiao Tong University (SJTU), Shanghai, China (email: yynie408@gmail.com, luozhe2007@hotmail.com, gulixu@sjtu.edu.cn; telephone: +86-02162933250; fax: +86-02162933250).

Junfeng Cai is with Department of Cardiac Surgery, Ruijin Hospital, Shanghai, China (email: lonlon_cn@hotmail.com).

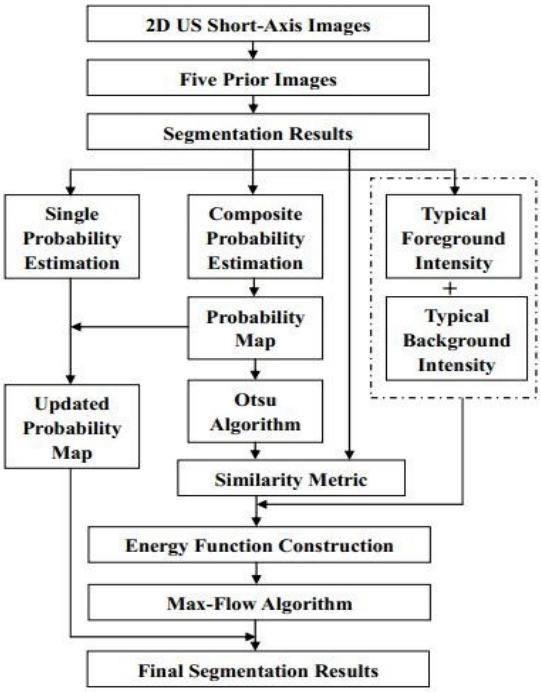

Figure 1. Flow chart for our aortic valve segmentation algorithm

1) Leaflet motion: the leaflets of the aortic valve have a relatively intense change of position and shape during the valve opens and closes in a cardiac cycle.
2) Artifacts: the heavy calcification of the leaflets causes large shadowing artifacts. It's hard to detect artifacts previously to guarantee they won't interfere with postoperative processing.
3) Speckle noise: speckle noise, which is inherent to US image, is the major difficulty when processing and analyzing US image.
4) Acquisition on polar coordinates: image data are collected on polar coordinates, which leads to a nonuniform inter-sampling space.

Manual segmentation by experts of US image is prohibitively time consuming and tedious, which have forced implementation of semi-automatic or automatic algorithms. The literature allocated to methods for echocardiography segmentation is extensive. Yan et al. [7] applied level set method to detect echocardial boundary using an improved fast marching method reducing the influence of noise, which has qualitative results and lacks of quantitative evaluation. Qian et al. [8] introduced a segmentation method for rat cardiac US images of short-axis view containing large dropout regions. They originally proposed tunneling descent for active contour evolution that can overcome spurious local minima using an explicit stopping rule. Carneiro et al. [9] proposed a

segmentation method for left ventricle of US based on deep neural network and efficient searching algorithms. Their algorithm is robust to imaging conditions and simplifies the complicated search process of pattern recognition. However it requires a large set of training images. Schneider et al. [2] designed a mitral annulus segmentation algorithm using graph cut, and the only input of this algorithm is the user-specified point which makes it operator-independent, but it just takes closed mitral valve into consideration.

Automatic method to delineate the aortic valve of transesophageal echo was presented in [5], where the aortic valve of short-axis view is segmented based on continuous max-flow (CMF) approach [10], which constructs energy function using prior information (image gradient, probability estimation, etc.) coming from the first three images in one cardiac cycle. The position and shape of aortic valve vary in a large range during a cardiac cycle resulting from its open and close. However, the first three images only represent part of aortic valve variation during the whole cardiac cycle, which makes the segmentation accuracy compromised. In addition, only composite probability estimation (CPE) is constructed using the first three images.

Inspired by the previous work in [5], this paper proposes a segmentation algorithm taking more prior US images evenly spanning a cardiac cycle into account and constructing both CPE and single probability estimation (SPE). This algorithm first gets CPE and SPE over the 5 prior images based on both intensity and distance to the corresponding centroid, then constructs energy function for the current input image, followed by a Graphic Processing Unit (GPU) [11] accelerated CMF approach to obtain segmentation results.

The outline of the paper is shown as below. Section II describes the details of the algorithm, as shown is Fig. 1. Section III presents three experiments of the algorithm, then followed by the conclusion in Section IV.

II. METHODLOGY

A. Continuous max-flow image segmentation

The aortic valve segmentation algorithm extensively makes use of CMF approach [10], in which the image segmentation with two regions can be described as a minimization problem of an energy function [12]:

$$\arg\min_{\lambda\in[0,1]} E(\lambda)=\int_{\Omega}(1-\lambda(x))C_s(x)dx+\int_{\Omega}\lambda(x)C_t(x)dx+\int_{\Omega}C_p(x)\left|\nabla\lambda(x)\right|dx \quad (1)$$

where $\lambda(x)\in[0,1]$ is a labeling function which labels image pixel x as foreground or background, $C_s(x)$ and $C_t(x)$ are regional properties that can be interpreted as penalties to assign a pixel as foreground and background based on image properties respectively, $C_p(x)$ is boundary property which represents a penalty for a discontinuity between two pixels, and $\left|\nabla\lambda(x)\right|$ is the total variation of the labeling function.

Compared with classic graph-cut based methods [13, 14], CMF algorithm can improve the segmentation accuracy with its ability of avoiding grid bias, and can be implemented and parallelized by graphics card.

B. Probability Estimation

Segmentation of US images primarily relies on image gradients or differences in intensity distributions between the foreground and background [2, 15, 16]. However, owing to the rapid motion of aortic valve leaflets and the low quality of US image, it is hard to utilize the information about gradients and differences in intensity distributions. Considering that low intensity pixels near the centroid of prior segmentation are more likely to be foreground (pixels corresponding to the leaflets), while high intensity pixels far from the centroid are more likely to be labeled as background, intensity and distance to the corresponding centroid are both used to construct probability estimation function. Compared with Pencilla et al. [5], this paper takes more prior US images evenly spanning a cardiac cycle into account and constructs not only CPE but also SPE, which contains prior probability distribution information of the prior image best matching the current input image.

We select 5 prior images evenly spanning a cardiac cycle with aortic valve manually segmented by an expert. Based on the segmentation of the 5 prior images, CPE is generated by calculating the conditional probability [3] of a pixel identified as foreground based on intensity and distance to the centroid (Fig. 2(a)), which is the geometry mean of segmented regions in all the prior images, as shown in Equation (2):

$$P(x)=P(F(x)\mid R(x),\ I(x))=\frac{1}{n}\sum_{i=1}^{n}\frac{P(F_i(x)\mid R(x),\ I(x))}{P(R(x),\ I(x))} \quad (2)$$

where $P(F_i)$ is the probability of a pixel belonging to the foreground, $P(R,I)$ is the probability of a pixel, whose distance to centroid is R and intensity is I, belonging to the foreground, and n is the number of prior images (In this study, n was set to 5).

Besides CPE, SPE is calculated for each prior image (Fig. 2(b)), which uses the true centroid of each prior image by Equation (3):

$$P_i(x)=P(F(x)\mid R(x),I(x))=\frac{P(F\cap R(x),I(x))}{P(R(x),I(x))} \quad (3)$$

where $P_i(x)$ is the probability function of i-th prior image (i=1, 2, 3, 4, 5).

In addition, for each prior image i, its typical foreground I_F^i and background intensity I_B^i, which can represent corresponding foreground and background intensities, are calculated respectively using Equation (4) and (5):

$$I_F^i=\sum_{p\in F}I(p)*P_{I(p)}^{F} \quad (4)$$

$$I_B^i=\sum_{p\in B}I(p)*P_{I(p)}^{B} \quad (5)$$

where F and B respectively represent the foreground region and the background region, P_I^F and P_I^B are respectively the probability of intensity I in foreground and background region, and $I(p)$ is the intensity of pixel p.

In this study, 5 groups of I_F^i and I_B^i are acquired.

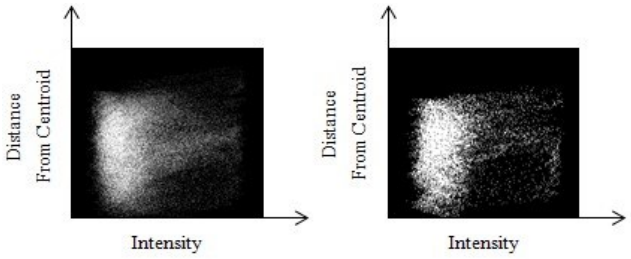

(a) (b)

Figure 2. Probability estimation. (a) Composite probability estimation; (b) Single probability estimation.

C. Energy Function Construction

The probability map of current input image is first acquired using CPE, as shown in Fig. 3, followed by Otsu algorithm to get an optimal threshold. Then pixels with the intensity below the threshold are removed, and the remainder comprise a target region A with a centroid C. Afterwards, a similarity metric (SM) is calculated to find out the prior image best matching the current input US image, as defined in Equation (6):

$$SM_i = \sum_{p \in A} \sqrt{(D_p - D_p^i)^2 + (I_p - I_p^i)^2} \quad (6)$$

where D_p is the distance from pixel p in A to C, and D_p^i is the distance from corresponding pixel p of prior image i to its own centroid, I_p is the intensity of p, and I_p^i is the intensity of p in prior image i.

Then, the probability map of current input image is updated by SPE of the best matching prior image PI_M, and I_F and I_B of PI_M are used to construct the energy function for the current input image of short-axis view by Equations (7)-(9):

$$C_s(x) = |I_x - I_F| \quad (7)$$
$$C_t(x) = |I_x - I_B| \quad (8)$$
$$C_p(x) = 0.5 \quad (9)$$

where x is the position of a pixel, $C_s(x)$ and $C_t(x)$ are the regional items respectively representing the foreground and background, $C_p(x)$ is the boundary item, and I_F and I_B are the corresponding typical foreground and background intensity of the prior image PI_M.

Afterwards, GPU accelerated CMF approach is employed to get an initial segmentation result. The final result is obtained after the initial result is multiplied by the updated probability map.

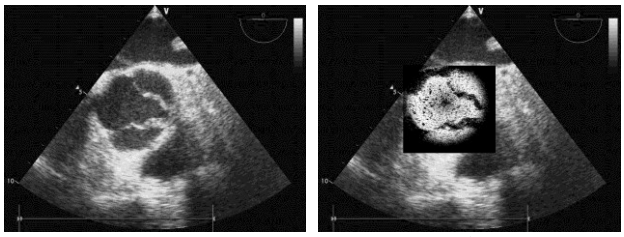

(a) (b)

Figure 3. (a) the current input image; (b) the probability map of the current input image.

III. Experiments

To evaluate the proposed algorithm, 3 subjects each with 90 short-axis cardiac US sequences were used and a total of 270 images (640*480) were segmented. The image data were acquired from Ruijin Hospital with a GE Vivid 7 US machine(GE M3S 1.5 MHz Matrix Phased Array Adult Cardiac Probe), and we performed our experiments under

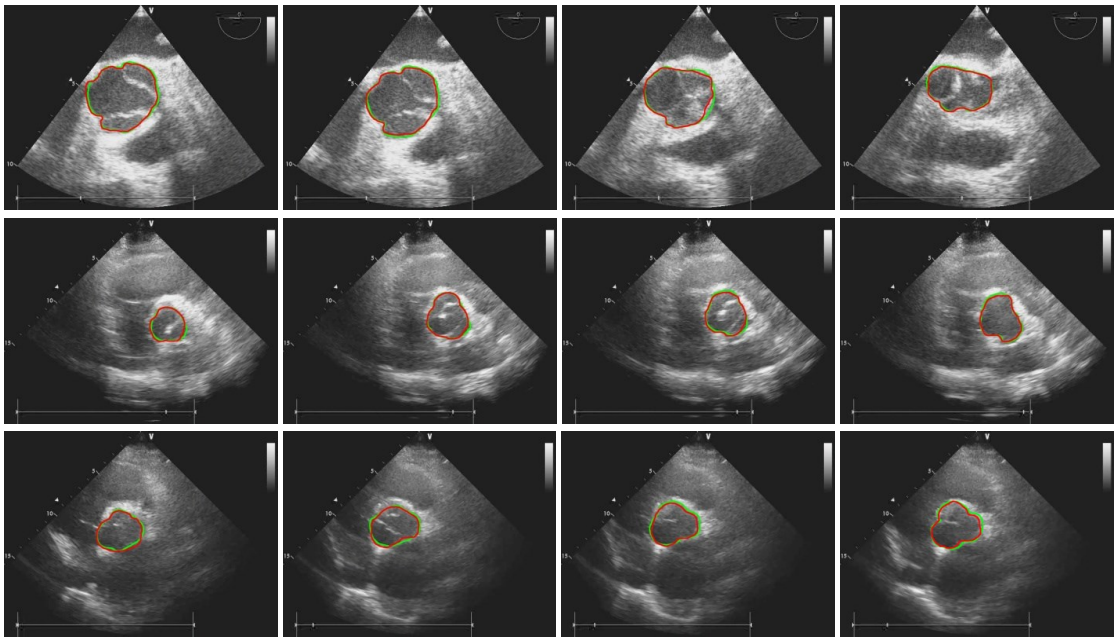

Figure 4. Segmentation results showing four points in the cardiac cycle for one human (first row) and two swine (second row and third row). Green line depicts ground truth. Red line represents the contour extracted by the algorithm. First row from frames 32, 35, 42 and 55; Second row from frames 76, 80, 83 and 87; Third row from 1, 9, 11 and 18.

Windows XP on an Intel Core i7 computer with NVIDIA GeForce GTX 560 graphics card with 1 GB display memory and 256 bit data width. For evaluation purpose, the automatic segmentation results were compared with the corresponding ground truth. Fig. 4 shows the segmentation results.

To obtain quantitative performance assessment of the proposed method, a scoring system consisting of three error measures including Average Symmetric Contour Distance (ASCD), Dice Metric (DM) and Reliability of the algorithm was employed [17, 18].

Low ASCD with high DM means high similarity between the automatic segmentation result and the ground truth, indicating that the automatic segmentation result has good correlation with manual segmentation result by the expert. $R(d)$ measures the reliability of the algorithm. The overall performance of the algorithm is summarized in Table 1. Fig. 5 and Fig. 6 respectively depict the ASCD and DM as a function of time, i.e., throughout the cardiac cycle. Fig. 7 depicts R as a function of d.

Table 1. ASCD, DM, Reliability of the algorithm (in pixels), and processing time per frame; ASCD and DM are expressed as mean ± standard deviation.

Items	ASCD	DM	Reliability (d = 0.95)	Time per frame (ms)
Our method	1.79±0.46	0.96±0.01	0.84	39.23±5.02

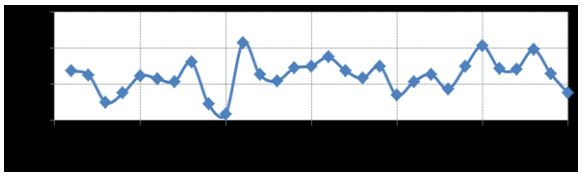

Figure 5. Example of variation of ASCD as a function of the time step

Figure 6. Example of variation of DM as a function of the time step

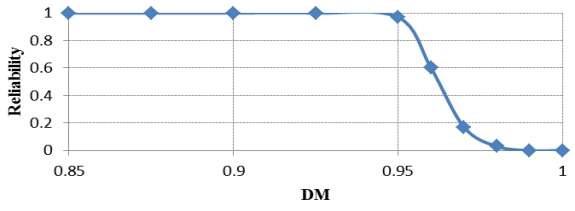

Figure 7. Reliability for the proposed algorithm.

IV. Conclusion

This paper investigated a robust algorithm detecting the aortic valve in cardiac US sequences of the short-axis view in approximately real time. The solution is obtained using probability estimation and GPU accelerated CMF approach. Corresponding evaluations over 270 images acquired from 3 subjects demonstrated that the segmentation results correlate well with manual segmentation results by the expert. Compared with Pencilla et al. [5], the proposed method improves accuracy and reduces computational time. In the future, our research will focus on the segmentation of long axis aortic root structure.

References

[1] R. R. Moss, *et al.*, "Role of Echocardiography in Percutaneous Aortic Valve Implantation," *JACC: Cardiovascular Imaging,* vol. 1, pp. 15-24, 2008.

[2] R. J. Schneider, *et al.*, "Mitral annulus segmentation from 3D ultrasound using graph cuts," *Medical Imaging, IEEE Transactions on,* vol. 29, pp. 1676-1687, 2010.

[3] K. Masuda, *et al.*, "Three dimensional motion mechanism of ultrasound probe and its application for tele-echography system," in *Intelligent Robots and Systems, 2001. Proceedings. 2001 IEEE/RSJ International Conference on*, 2001, pp. 1112-1116.

[4] C. H. Huber, *et al.*, "Ultrasound navigation through the heart for off-pump aortic valved stent implantation: new tools for new goals," *Journal Information,* vol. 11, 2004.

[5] P. Lang, *et al.*, "Feature identification for image-guided transcatheter aortic valve implantation," in *SPIE Medical Imaging*, 2012, pp. 83162X-83162X-14.

[6] J. M. B. Dias and J. M. N. Leitao, "Wall position and thickness estimation from sequences of echocardiographic images," *Medical Imaging, IEEE Transactions on,* vol. 15, pp. 25-38, 1996.

[7] J. Yan and T. Zhuang, "Applying improved fast marching method to endocardial boundary detection in echocardiographic images," *Pattern Recognition Letters,* vol. 24, pp. 2777-2784, 2003.

[8] X. Qian, *et al.*, "Segmentation of rat cardiac ultrasound images with large dropout regions," in *Computer Vision and Pattern Recognition Workshop, 2006. CVPRW'06. Conference on*, 2006, pp. 93-93.

[9] G. Carneiro, *et al.*, "Robust left ventricle segmentation from ultrasound data using deep neural networks and efficient search methods," in *Biomedical Imaging: From Nano to Macro, 2010 IEEE International Symposium on*, 2010, pp. 1085-1088.

[10] J. Yuan, *et al.*, "A study on continuous max-flow and min-cut approaches," in *Computer Vision and Pattern Recognition (CVPR), 2010 IEEE Conference on*, 2010, pp. 2217-2224.

[11] M. Rajchl, *et al.*, "Fast interactive multi-region cardiac segmentation with linearly ordered labels," in *Biomedical Imaging (ISBI), 2012 9th IEEE International Symposium on*, 2012, pp. 1409-1412.

[12] J. Yuan,, *et al.*, "A Continuous Max-Flow Approach to Potts Model," *ECCV'10 Proceedings of the 11th European conference on Computer vision,* part VI , pp. 379-392, 2010.

[13] Y. Y. Boykov and M. P. Jolly, "Interactive graph cuts for optimal boundary & region segmentation of objects in ND images," in *Computer Vision, 2001. ICCV 2001. Proceedings. Eighth IEEE International Conference on*, 2001, pp. 105-112.

[14] Y. Boykov and V. Kolmogorov, "An experimental comparison of min-cut/max-flow algorithms for energy minimization in vision," *Pattern Analysis and Machine Intelligence, IEEE Transactions on,* vol. 26, pp. 1124-1137, 2004.

[15] J. A. Noble and D. Boukerroui, "Ultrasound image segmentation: A survey," *Medical Imaging, IEEE Transactions on,* vol. 25, pp. 987-1010, 2006.

[16] P. Lang, *et al.*, "Towards Model-Enhanced Real-Time Ultrasound Guided Cardiac Interventions," pp. 89-92, 2011.

[17] T. Heimann, *et al.*, "Comparison and evaluation of methods for liver segmentation from CT datasets," *Medical Imaging, IEEE Transactions on,* vol. 28, pp. 1251-1265, 2009.

[18] I. Ben Ayed, *et al.*, "Max-flow segmentation of the left ventricle by recovering subject-specific distributions via a bound of the Bhattacharyya measure," *Medical Image Analysis,* vol. 16, pp. 87-100, 2012.